

Electronic Structure and Chemical Bonding within MgB_2 and Related Borides from First Principles

Samir F. Matar

Institut de Chimie de la Matière Condensée de Bordeaux (ICMCB), CNRS, Université Bordeaux 1, 87 Avenue du Dr. Albert Schweitzer, F-33608 Pessac Cedex, France

Reprint requests to S. F. Matar. E-mail: matar@icmcb-bordeaux.cnrs.fr

Z. Naturforsch. **2008**, *63b*, 673–680; received November 8, 2007

Dedicated to Professor Gérard Demazeau on the occasion of his 65th birthday

The electronic structures of actual and hypothetical binary borides AB_2 ($A = \text{Al, Mg, Li, Be, Ca}$) and of mixed hypothetical phases $A'\text{MgB}_4$ ($A' = \text{Al, Li}$) are obtained and analyzed within the density functional theory using pseudo-potential and all-electron methods (VASP and ASW) in order to address the changes in the electronic structure within the high-temperature superconductor MgB_2 by modeling isoelectronic and n/p -doping effects. From the properties of quantum mixing between respective valence states and of chemical bonding we propose an analysis of the high-temperature superconductivity within the two models, the classical one of Bardeen, Cooper and Schrieffer (BCS) and the hole superconductivity model, which is based on experimental and calculated results from the literature.

Key words: Density Functional Theory, Borides, VASP, ASW, BCS and Hole Superconductivity

Introduction

Several early experimental [1–3] and theoretical [4] investigations of the large family of borides (alkali, alkaline earth, rare earth and actinide elements) were motivated by the electronic (*e. g.* electron beam source) and physical (*e. g.* hard, refractory) properties. However the unexpected superconductivity at $T_C = 40$ K for MgB_2 [5–6] has initiated a renewed interest in the study of 2D [7, 8] and 3D [4, 9] borides in order to assess such a peculiar behavior on the basis of the low dimensionality, electron-phonon coupling and bonding properties of these materials.

The electronic band structure characteristics of MgB_2 are well established [8]. After a short description in the context of chemical interactions, we focus in this work on the changes of chemical bonding within MgB_2 by confronting its properties with those of two other 2D diborides adopting the same structure, the hypothetical LiB_2 (one valence electron less) and AlB_2 (one extra electron) as well as within their hypothetical 1:1 $A'\text{MgB}_4$ ($A' = \text{Al, Li}$) mixtures with the help of density functional quantum theory (DFT) [10, 11]. Further we consider two other hypothetical isoelectronic systems, BeB_2 and CaB_2 , when discussing the relationship between the band and

crystal structure *versus* the superconducting behavior of MgB_2 .

Two DFT-based methods have been used: the pseudo-potential plane waves method for full geometry optimizations (VASP code [12, 13]) and the all-electron augmented spherical wave ASW method [14, 15] for a full account of the band structure and the chemical bonding properties. Indeed, the physical properties of the electron system and their changes are ruled by the chemical bonding within such compounds, namely the ionic-covalent bond between boron and the metal on one hand and within the boron sublattice on the other hand.

Geometry Optimization Methodology and Computational Details

The first step of the full geometry optimization is carried out using the VASP code [12, 13]. The ion-electron interaction is treated by the ultra-soft pseudo potentials (US-PP) of Vanderbilt [16] whereas the electron-electron interaction is described in the local density approximation (LDA) of DFT by the Ceperley-Alder exchange-correlation potential [17], parameterized by Perdew and Zunger [18]. In the plane wave pseudo-potential approach, the rapid variation of the

a)	AB ₂ syst.	AlB ₂	MgB ₂	<i>LiB₂</i>	<i>AlMgB₄</i>	<i>LiMgB₄</i>
	<i>a</i> (Å)	3.01 / 2.97	3.08 / 3.03	2.93	2.99	2.98
	<i>c/a</i>	1.084 / 1.089	1.12 / 1.13	1.13	2.21	2.28
	<i>V</i> (Å ³)	25.60 / 24.93	28.45 / 27.25	24.81	51.3	52.42
	<i>B</i> ₀ (kbar)	210	174	151		
	<i>d</i> _{A-B} (Å)	2.35	2.45	2.37		
	<i>d</i> _{B-B} (Å)	1.71	1.75	1.69		
	<i>r</i> _A ^o (Å)	1.43	1.60	1.55		
	<i>χ</i> _A	1.61	1.31	0.98		
b)	AB ₂ syst.	<i>BeB₂</i>	MgB ₂	<i>CaB₂</i>		
	<i>a</i> (Å)	2.89	3.08 / 3.03	3.13		
	<i>c/a</i>	0.96	1.12 / 1.13	1.26		
	<i>V</i> (Å ³)	20.75	28.45 / 27.25	33.17		
	<i>B</i> ₀ (kbar)	218	174	136		
	<i>d</i> _{A-B} (Å)	2.21	2.45	2.66		
	<i>d</i> _{B-B} (Å)	1.66	1.75	1.81		
	<i>r</i> _A ^o (Å)	1.11	1.60	1.97		
	<i>χ</i> _A	1.57	1.31	1.0		

Table 1. Crystal parameters (italics) resulting from the geometry optimizations on the different AB₂ systems studied in this work: a) change of valence of A (trivalent to monovalent) and mixtures of A elements; b) change of chemical nature of divalent A. Phases with formulae in italics are hypothetical. Where available, experimental data are in straight letters. Note that $\chi_B = 2.04$.

potential near the nuclei is avoided by substituting the all electrons Hamiltonian with a smoother pseudo-Hamiltonian which reproduces the valence energy spectrum. The use of pseudo-potentials allows a considerable reduction of the necessary number of plane waves per atom so that force and full stress tensors can be readily calculated and used to relax atoms into their ground state. A conjugate-gradient algorithm is used to relax the ions of the different structural setups of the AB₂ (A = Li, Mg, Be, Ca, Al) and A'MgB₄ (A' = Al, Li) hexagonal phases. The optimization of the structural parameters was performed until the forces on the atoms are less than 0.02 eV Å⁻¹, and all stress components were less than 0.003 eV Å⁻³. All calculations were performed by using an energy cut-off of 321.44 eV for the plane wave basis set. The tetrahedron method with Blöchl corrections [19] for conducting systems was applied for both geometry relaxation and total energy calculations. Brillouin-zone integrals were approximated using the special *k*-point sampling of Monkhorst and Pack [20].

The AlB₂-type hexagonal structure (space group *P6/mmm*) of MgB₂ has one formula unit per cell. With Mg at the origin (0,0,0) the structure is characterized by a graphite-like two dimensional network (1/3, 2/3, 1/2 and 2/3, 1/3, 1/2), with the boron layers stacked perpendicular to the *c* axis. The boron atoms form trigonal prisms around the metal atoms.

Table 1 summarizes the results of the geometry optimizations. A confrontation with experimental values for the existing systems, AlB₂ and MgB₂, shows a slight underestimation of the lattice constants (*a*, *c/a* and resulting *V*). This is a common feature of the LDA

based on the homogeneous electron gas distribution. However, this provides some confidence in the computed lattice constants for the other hypothetical systems. The trends are those expected from the changes in atomic radii of the elements A (Table 1). The exception for the hypothetical lithium diboride system is likely due to the fact that Li is totally ionized so that the ionic radius of Li⁺ of 0.68 Å fits better to the observed lattice constant trend. Another quantity worth addressing within the diboride series in Table 1a is the bulk module *B*₀ obtained from a Birch equation of state non-linear fit of the quadratic *E*(*V*) curves. The *B*₀ values are close to those of 2D systems such as graphite with the largest magnitude for the most covalent system, *i. e.* AlB₂, and the smallest for LiB₂. On the side of isoelectronic systems to MgB₂, *i. e.* hypothetical BeB₂ and CaB₂ (Table 1b), the trend of the largest bulk module for the most covalent BeB₂ is also confirmed, and its magnitude is only slightly larger than for AlB₂. This is also stressed by the Pauling electronegativity values χ_A added to Table 1. For the 1 : 1 mixtures in Table 1a, for which the purpose was to obtain equilibrium lattice constants for later use in all electrons calculations, we have not accounted for possible effects of structural disorder such as in a solid solution. That would require creating large super cells with random distribution of the atoms, as well as the use of other computational tools such as the coherent potential approximation (CPA) [21]. Nevertheless, the optimized lattice constants for the ordered structures were used for assessing the changes in the boron sublattice as discussed below. Finally, within the divalent isoelectronic diboride series in Table 1b, the decrease of χ_A is con-

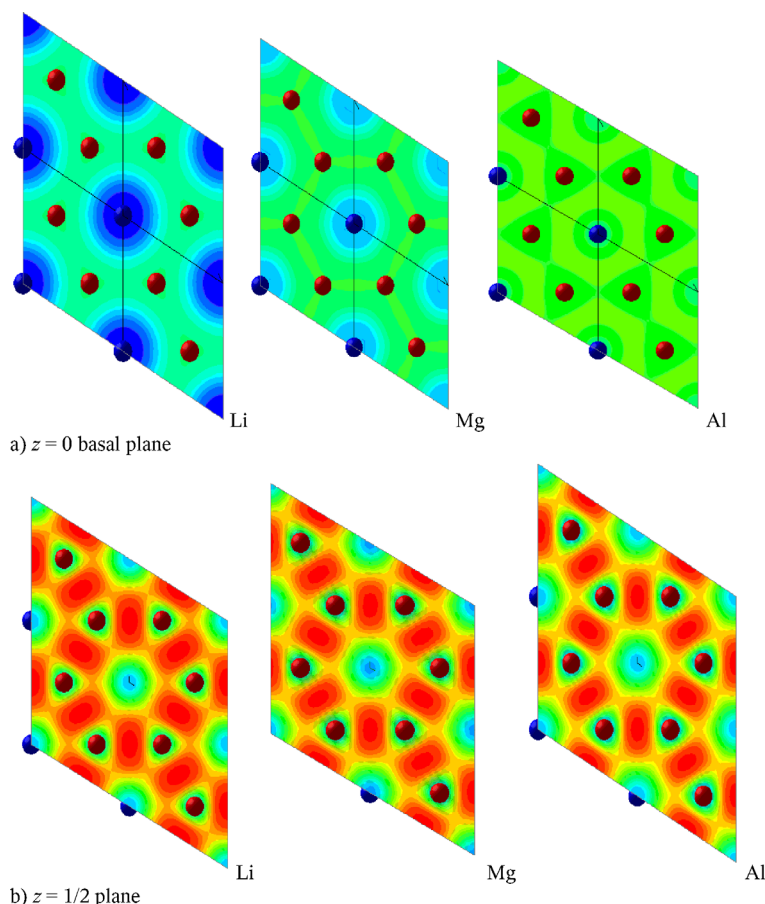


Fig. 1. (Color online) Electron localization function ELF contours for AB_2 ($A = \text{Li}, \text{Mg}, \text{Al}$) showing 4 cells. Blue, green and red contours are for no ($\text{ELF} = 0$), free electron gas ($\text{ELF} = 1/2$) and strong ($\text{ELF} = 1$) electron localization, respectively.

comitant with the increase of the atomic radii and with the interatomic distances and the volume.

Besides the geometry optimization, the results allow extracting a first description of the electron localization function ELF [22] based on a comparison of the actual localization normalized with respect to the free electron distribution for which one considers the unit-less ELF at a value of $1/2$. For the actual chemical system, ELF numbers vary from 0 for no localization to 1 for full localization. Within the diboride systems this provides contour plots which are shown for the metal and boron planes within the three AB_2 systems, $A = \text{Li}, \text{Mg}, \text{Al}$, in Fig. 1. For the sake of a significantly clear illustration, projections for four adjacent cells are given orthogonal to the basal plane. At $z = 0$, describing the metal containing plane, the picture of the tendency of covalence becomes more pronounced along the series with the smearing of the charge within AlB_2 , whereas LiB_2 is found to behave as the “most ionic” system. MgB_2 is found half-way. At $z = 1/2$ a main feature is

observed for the concentration of the contours around the boron dumbbell-like “ B_2 ” entity with little expansion towards the metal atoms. From the intensity of the contours in between boron atoms, the strongest B–B bonding seems to characterize LiB_2 ; this is further confirmed by the chemical bonding analysis in the following sections (see Fig. 5b).

Results of All-electron Calculations

Using the structural parameters obtained from the full geometry optimization of the boride systems (Table 1), all-electron calculations with the ASW method [14, 15] were carried out for the band structure, the Fermi surfaces, the density of states (DOS) and the properties of chemical bonding using the overlap population analysis (COOP) [23]. In the ASW method the wave function is expanded in atom-centered augmented spherical waves, which are Hankel functions and numerical solutions of Schrödinger’s equation, re-

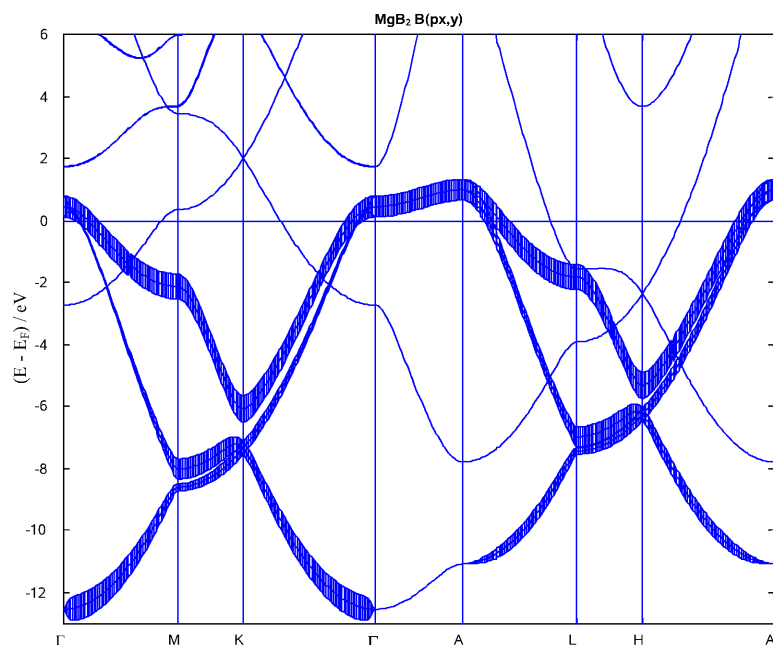


Fig. 2. Band structure of MgB₂ along major directions of the hexagonal Brillouin zone. Fat bands show the weighting with boron $p(x, y)$ orbitals; other thin bands are for B(p_z) (see text).

spectively, outside and inside the so-called augmentation spheres. In order to optimize the basis set, additional augmented spheres with zero core (empty spheres, ES) were placed at carefully selected interstitial sites. The choice of these sites as well as the augmentation radii were automatically determined using the sphere-geometry optimization algorithm [24]. ES are especially necessary in open structures such as that of the 2D-AlB₂ type; they receive charge residues from the actual atomic spheres. All valence states were treated as band states. The completeness of the valence basis set was checked for charge convergence. The self-consistent field calculations were run to a convergence of $\Delta Q = 10^{-7}$, and the accuracy of the method is in the range of about 1 meV regarding energy differences. Like above the effects of exchange and correlation are treated within the LDA using the same parameterization scheme.

Band structure

The band structure of MgB₂ along main symmetry lines of the hexagonal Brillouin zone (BZ) is shown in Fig. 2. It is very similar to the one previously obtained by An and Picket [8]. We here focus on the chemical roles of the orbitals involved in the bonding. Two partially filled bands crossing the Fermi level (see the lines along the Γ -A direction), strongly weighted by

boron $p(x, y)$ states, are shown in fat lines. Within LiB₂ and AlB₂, these bands are, respectively, further raised above and lowered below the Fermi level as one may expect from the electron occupations of Li (one electron less) and Al (one extra valence electron) *versus* Mg. In this context the change of the band structure within a sub-stoichiometric Al_{0.9}B₂ single crystal was recently addressed by Burkhardt *et al.* [25] who found a hole conductivity experimentally, and confirmed the trend with electronic band structure calculations showing that the B bands are raised above the Fermi level. These bands arise from both π - and σ -type bands. It has been suggested that the high- T_C superconductivity in MgB₂ arises from the high sensitivity of the partially empty σ bands to bond stretching modes [8] so that a gap opening lifts the degeneracy of all the σ states at the Fermi level along the Γ -A direction due to the electron-phonon coupling. In the coordinate system in which the graphite-like boron layer is on the xy plane (*cf.* Fig. 1), the group of B-B orbitals leading to the partially filled π bands are the π_z and π_z^* orbitals, and those leading to the partially filled σ bands are the σ_x and π_y^* orbitals. The π bands of a single boron layer (with one electron per boron atom transferred to the boron layer from Mg) are the same as those of a single graphite sheet. The Coulombic attraction between the negatively charged boron sheets and the Mg²⁺ cations preferentially lowers the whole π bands with respect

to the filled σ bands because the π electrons are closer to the Mg²⁺ cations than are the σ electrons. Consequently, the two highest filled σ bands become partially empty.

At this point one needs to address the aspect of the specific role of Mg²⁺ cations in the electron transfer from the σ to the π^* bands. This has been checked with additional calculations on the hypothetical iso-electronic systems BeB₂ and CaB₂. The lattice parameters for the geometry optimized systems provided in Table 1b point to intermediate values for the actual MgB₂ boride especially for the c/a ratio and the volume: From this BeB₂ with the smallest c/a ratio would lead to an unstable layered structure whereas CaB₂ with the largest volume and c/a ratio leads to an extended diffuseness of Ca 4s/4p orbitals as compared to the Mg 3s/3p ones. Thus the overlap of the Mg 3s/3p orbitals with the 2p π orbitals of the adjacent boron layers is essential for the electron transfer from the σ bands to the π^* bands in MgB₂.

Density of states and chemical bonding

Fig. 3 gives for the three diboride AB₂ systems, A = Li, Mg, Al, the total and partial DOS (PDOS) for each constituent. From the total DOS, the trend is a decreasing expansion of the valence band and an increase of $n(E_F)$ along the series. This is mainly due to changes in the position and intensity of boron PDOS which are most affected by the changes within the metal sublattice. At the Fermi level the presence of the boron states becomes more pronounced from AlB₂ to “LiB₂”. In the band structure picture this corresponds with the raising of the B bands from below E_F (AlB₂) to above E_F for LiB₂ with hole creation. The low intensity A PDOS are broad and extend through the VB. The similar skylines with the B PDOS are a signature of the chemical bonding which is detailed below. The narrowing of the band is concomitant with a peaking of the boron PDOS observed at ≈ -0.5 eV in hypothetical lithium boride which is the most ionic (*cf.* Fig. 1). This can be better explained using bonding criteria within the COOP scheme [23].

Fig. 4 shows in two panels the character of the chemical bond for the A–B and B–B interactions, respectively, for the series A = Al, Mg, Li. Positive COOP values point to bonding states whereas negative values are relevant to anti-bonding ones. In the top panel the comparison of the three kinds of

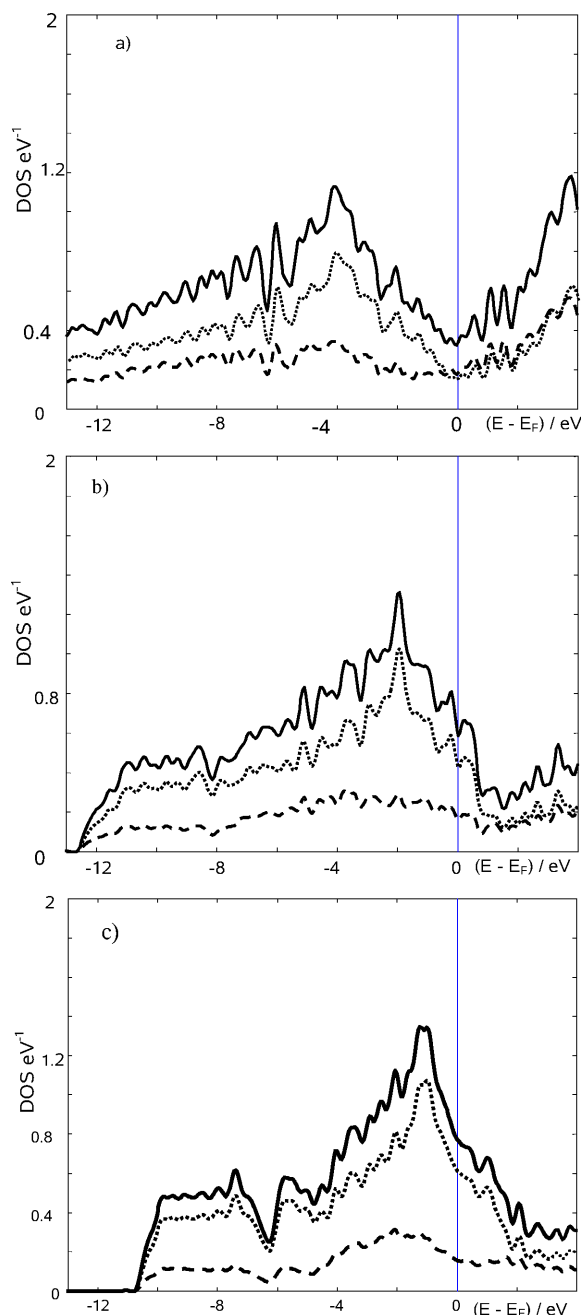


Fig. 3. Total (full line), and partial DOS for AB₂ (dashed and dotted lines for A and B). a) A = Al, b) A = Mg, c) A = Li.

A–B bonds points to larger bonding contributions for the Al–B states especially in the lower part of the valence band, *i. e.* where the Li–B interaction is at its lowest. The strength of the Mg–B interaction is intermediate between that of the two other metals.

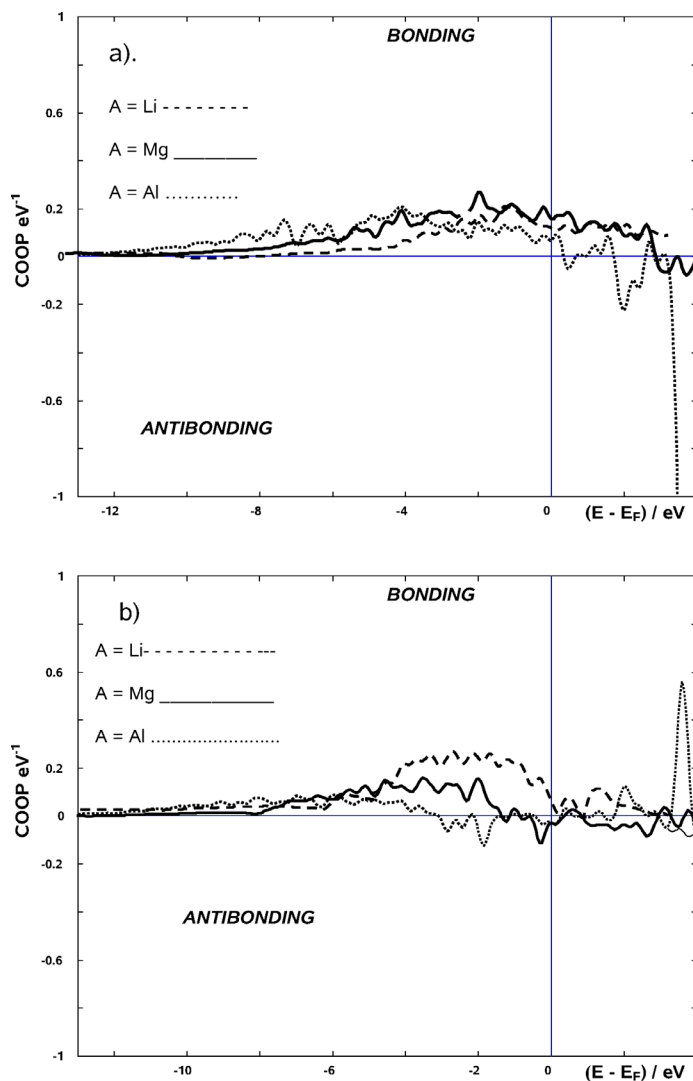


Fig. 4. AB_2 : COOP for a) A–B and b) B–B interactions for A = Al, Mg, Li.

This is observed too in the lower panel where the B–B interactions are shown. Another feature worth mentioning is the maximum exhibited for the B–B bond in the lithium compound at ≈ -2 eV. This feature which was already pointed out while discussing the ELF (Fig. 1) is concomitant with the large DOS peak observed for the B states in Fig. 3. The bonding within the boron sublattice is clearly the strongest for the hypothetical lithium compound. On the other hand let us note that whatever the boride system, the metal-boron and boron-boron interactions are respectively bonding and anti-bonding at the Fermi level.

Mixtures of borides

In a further step, we studied the effects of mixtures by employing double cells constructed along the hexagonal c axis (*cf.* Table 1). The resulting unit cell becomes $\text{Mg}(A)\text{B}_4$ where A for instance can be Al or Li. If $A = \text{Mg}$, the pristine MgB_2 cell is reproduced, but simply doubled. Fig. 5 shows the boron DOS for the three superlattices AlMgB_4 , Mg_2B_4 and LiMgB_4 . $n(E_F)$ are the largest and the lowest for the lithium and the aluminium cases, respectively, as the study of the pure hypothetical compounds has already shown. The other feature worth underlining is that whereas the narrowest band of boron is observed for the lithium case,

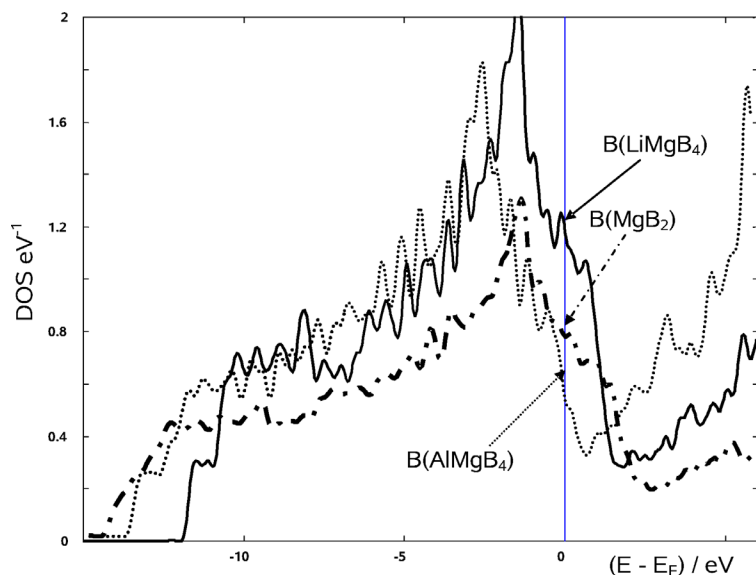


Fig. 5. Comparative DOS of the boron sublattice in the double Mg(A)B₄ (A = Al, Mg, Li) phases.

the broadest one is not for AlMgB₄ but for MgB₂ itself. Further, the substitution of Li for Mg in MgB₂ leads to a large enhancement of the B DOS peak just below the Fermi level. This indicates a larger bonding within B–B in LiMgB₄, with the lithium introducing an enhanced ionic character within the boride system.

Discussion

From the presented results, many points can be highlighted when comparing the chemical bonding approaches of the boride systems. It has been shown that upon moving from AlB₂ to LiB₂ through MgB₂, the following trends are observed:

- (i) an enhancement of the ionicity of the chemical bonding (ELF plots, Fig. 1),
- (ii) a narrowing of the boron valence band (Fig. 3),
- (iii) a strengthening of the chemical bond within the boron sublattice (and weaker metal-boron bonds) (Fig. 4),
- (iv) an enhancement of $n(E_F)$ likely to lead to an increase of the hole concentration.

This comparison should be made also in the framework of the electron-phonon or hole superconductivity mechanisms for explaining the superconducting behavior of MgB₂ [7, 8]. In simple terms we can say that

hole superconductivity is based on the pairing of hole carriers through their direct Coulomb interaction leading to superconductivity because of the momentum dependence of the repulsive interaction in the solid state environment [26]. In its essence the hole superconductivity mechanism is completely different from the conventional BCS (Bardeen-Cooper-Schrieffer) electron-phonon theory [27]. However, in the weak coupling regime, the predictions of the model of hole superconductivity are similar to those of the conventional BCS theory. In Mg_{1-x}Al_xB₂ [28] the electron doping leading to a decrease of the hole doping as x increases should increase T_C according to the hole superconductivity mechanism. However, an opposite behavior is observed, favoring the electron-phonon BCS theory which predicts a decrease of T_C as the density of states at the Fermi level decreases (Figs. 3, 5). Such a behavior can be understood through the McMillan-Hopfield expression giving the coupling parameter $\lambda = N(0)\langle I^2 \rangle / M\langle \omega^2 \rangle$ in which $N(0)$ is the density of states at the Fermi energy per spin and per atom, $\langle I^2 \rangle$, strongly correlated to the ionicity, is the averaged squared electron-ion matrix element, M is the atomic mass, and $\langle \omega^2 \rangle$ the phonon frequency (see ref. [29] for a recent use in boride superconductors).

Again, through the BCS theory we could expect, according to the calculations presented in this work, an increase of T_C in the Mg_{1-x}Li_xB₂ system thanks to an increase of both the density of states (Fig. 3) and the

enhanced ionicity of the chemical bond (Fig. 1) and an overall decrease of the mass. However, experimental results obtained in this system show an opposite trend which is rather consistent with the hole superconductivity mechanism [30]. Another argument in favor of the BCS theory for explaining the superconductivity behavior of MgB₂ is the effect of pressure on T_C , *i. e.* the decrease of T_C as the pressure increases contrary to what is predicted by the hole superconductivity mechanism [31].

Although there is a certain consensus for stating that the superconductivity of MgB₂ could be explained through the conventional BCS electron-phonon theory, the situation is far from clear. A real challenge is the preparation of single crystals of MgB₂ in order to have a well defined approach to the physical properties, but our experience has shown that this is

a tough task: MgB₂ is thermally not stable since it decomposes above 800 °C with loss of magnesium, leading to boron rich samples like MgB₄ [32]. Nevertheless by carefully controlling the rate of the decomposition of MgB₂, a magnesium-deficient boride Mg_{1-x}□_xB₂ (□ = vacancy) might be obtained which is likely to have both an increase of the hole doping and an enhanced density of states at the Fermi level.

Acknowledgements

I acknowledge fruitful discussions with Prof. Jean Etourneau (ICMCB, CNRS, University Bordeaux 1) at an early stage of development of the research in this topic. Computational facilities were provided within the intensive numerical simulation facilities network M3PEC-Mésocentre of the University Bordeaux 1, partly financed by the Conseil Régional d'Aquitaine and the French Ministry of Research and Technology.

-
- [1] J. Etourneau, R. Naslain, *J. Less-Common Met.* **1971**, *24*, 183.
- [2] J. Etourneau in *Inorganic Reactions and Methods*, Vol. 13, Eds.: J. J. Zuckerman, A. P. Hagen), VCH, Weinheim **1991**, pp. 167.
- [3] M. K. Blomberg, M. J. Merisalo, M. M. Korsukova, V. N. Gurin, *J. Alloys Comp.* **1995**, *217*, 23.
- [4] S. F. Matar, J. Etourneau, *Int. J. Inorg. Mater.* **2000**, *2*, 43.
- [5] S. L. Bud'ko, P. C. Canfield, *Phys. Rev. B* **2002**, *65*, 212501.
- [6] J. E. Hirsch, F. Marsiglio, *Phys. Rev. B* **2001**, *64* 144523.
- [7] J. Kortus, I. I. Mazin, K. D. Belashchenko, V. P. Antropov, L. L. Boyer, *Phys. Rev. Lett.* **2001**, *86*, 4656.
- [8] J. M. An, W. E. Pickett, *Phys. Rev. Lett.* **2001**, *86*, 4366.
- [9] A. Ammar, M. Ménétrier, A. Villesuzanne, S. F. Matar, B. Chevalier, J. Etourneau, G. Villeneuve, J. Rodriguez-Carvajal, H. J. Koo, A. I. Smirnov, M. H. Whangbo, *Inorg. Chem.* **2004**, *43*, 4974.
- [10] W. Kohn, L. J. Sham, *Phys. Rev. A* **1965**, *140*, 1133.
- [11] P. Hohenberg, W. Kohn, *Phys. Rev. B* **1965**, *136*, 864.
- [12] G. Kresse, J. Hafner, *Phys. Rev. B* **1993**, *47*, 558.
- [13] G. Kresse, J. Furthmüller, *Phys. Rev. B* **1996**, *54*, 11169.
- [14] A. R. Williams, J. Kübler, C. D. Gelatt, Jr., *Phys. Rev. B* **1979**, *19*, 6094.
- [15] V. Eyert, *The Augmented Spherical Wave Method – A Comprehensive Treatment*, Lect. Notes Phys. 719, Springer, Berlin, Heidelberg **2007**.
- [16] D. Vanderbilt, *Phys. Rev. B* **1990**, *41*, 7892.
- [17] D. M. Ceperley, B. I. Alder, *Phys. Rev. Lett.* **1980**, *45*, 566.
- [18] J. P. Perdew, A. Zunger, *Phys. Rev. B* **1981**, *23*, 5048.
- [19] P. E. Blöchl, O. Jepsen, O. K. Anderson, *Phys. Rev. B* **1994**, *49*, 16223.
- [20] H. J. Monkhorst, J. D. Pack, *Phys. Rev. B* **1976**, *13*, 5188.
- [21] A. M. N. Niklasson, J. M. Wills, M. I. Katsnelson, I. A. Abrikosov, O. Eriksson, B. Johansson, *Phys. Rev. B* **2003**, *67*, 235105.
- [22] A. D. Becke, K. E. Edgecombe, *J. Chem. Phys.* **1990**, *92*, 5397.
- [23] R. Hoffmann, *Angew. Chem.* **1987**, *99*, 871; *Angew. Chem. Int. Ed.* **1987**, *26*, 846.
- [24] V. Eyert, K.-H. Höck, *Phys. Rev. B* **1998**, *57*, 12727.
- [25] U. Burkhardt, V. Gurin, F. Haarmann, H. Borrmann, W. Schnelle, A. Yaresko, Y. Grin, *J. Solid State Chemistry* **2004**, *177*, 389.
- [26] J. E. Hirsh, *Phys. Rev. B* **2005**, *71*, 104522.
- [27] J. Bardeen, L. N. Cooper, J. R. Schrieffer, *Phys. Rev.* **1957**, *108*, 1175.
- [28] J. Q. Li, L. Li, F. M. Liu, C. Dong, J. Y. Xiang, Z. X. Zhao, *Phys. Rev. B* **2002**, *65*, 132505.
- [29] B. Wiendlocha, J. Tobola, S. Kaprzyk, *Phys. Rev. B* **2006**, *73*, 134522.
- [30] J. Y. Xiang, D. N. Zheng, J. Q. Li, P. L. Lang, H. Chen, C. Dong, G. C. Che, Z. A. Ren, H. H. Qi, H. Y. Tian, Y. M. Ni, Z. X. Zhao, *Phys. Rev. B* **2002**, *65*, 214536.
- [31] B. Lorenz, R. L. Meng, C. W. Chu, *Phys. Rev. B* **2001**, *64*, 012507.
- [32] J. Etourneau, private communication.